The Use of Satellite Imagery and Surface Pressure-Gradient Analysis Modified for Sloping Terrain to Analyze the Mesoscale Events Preceding the Severe Hailstorms of 2 August 1986

JOHN F. WEAVER

NOAA/NESDIS/RAMM Branch, Department of Atmospheric Science, Colorado State University, Fort Collins, Colorado

JAMES J. TOTH

Department of Atmospheric Science, Colorado State University, Fort Collins, Colorado*

(Manuscript received 10 April 1989, in final form 16 January 1990)

ABSTRACT

Conditions leading up to an outbreak of severe hailstorms in northeast Colorado are examined using satellite and surface data. A persistent mesoscale ridge of surface-high pressure, caused by outflow from a mesoscale-convective system, is seen to coincide with the occurrence of large hail which was confined to a narrow band extending nearly parallel to the Front Range of the Rocky Mountains. The development of the mesoscale ridge during its most intense stages is documented using a procedure that yields an approximate streamfunction for the surface geostrophic wind. Unlike alternatives over sloping terrain, this method is quick and can be adjusted to minimize the error over a limited portion of the analysis area.

1. Introduction

According to Purdom (1982) "the clouds and cloud patterns observed in a satellite image or animated series of images represent the integrated effect of ongoing dynamic and thermodynamic processes in the atmosphere." Although at first such a statement seems self-evident, it is often difficult to substantiate the apparent mesoscale features found on satellite imagery using conventional data analysis. One solution is to gather more data; another is to analyze the available data more carefully. This paper focuses on an improved analysis of the horizontal pressure gradient at the earth's surface.

Because horizontal gradients of pressure due to atmospheric factors can easily be masked by differences in pressure due to terrain height, surface pressures are generally reduced to sea level. Unfortunately, this standard method yields apparent gradients that can be significantly erroneous in areas where the surface is not at sea level (Sangster 1987, henceforth S87; Pielke and Cram 1987; Danard 1989). Furthermore, the use of a 12-h average temperature when calculating sea-level pressure tends to mask rapidly evolving mesoscale pressure gradients.

Analysis of altimeter settings, a popular and quick alternative, eliminates the reduction error over *flat* elevated terrain, but may introduce serious errors over *sloping* terrain (S87). As effectively described in S87, *adjusted* altimeter settings yield a much improved (yet still approximate) analysis of the surface horizontal pressure gradient over sloping terrain. A modification of the S87 technique is described in this paper. This somewhat simplified technique is suitable for either subjective or objective analysis of irregularly spaced surface observations, and can be tuned to minimize the adjustment error over a limited (mesoscale) portion of the analysis area.

A summary of the pressure-analysis technique used in this paper is given in section 2, while a detailed discussion is provided in the Appendix. In section 3, the technique is discussed as it applies to a specific place and time; namely, the Front Range of the Rocky Mountains in northeast Colorado on 1–2 August 1986. (See Fig. 1 for locations of topographic and geographic features.) In section 4, the surface analyses are used in conjunction with satellite imagery to document the development of a mesoscale air mass that played a key role in this severe weather case.

2. Pressure analyses over sloping terrain

As mentioned previously, there are significant problems in analyzing surface pressure gradients when the area of interest is in a region of sloping terrain. The problems are exacerbated when the area is experiencing

* Current affiliation: Department of Atmospheric Science, University of Wyoming, Laramie, WY 82071.

Corresponding author address: John F. Weaver, NOAA/NESDIS/RAMM Branch, Department of Atmospheric Science, CSU, CIRA Building, Foothills Campus, Fort Collins, CO 80523.

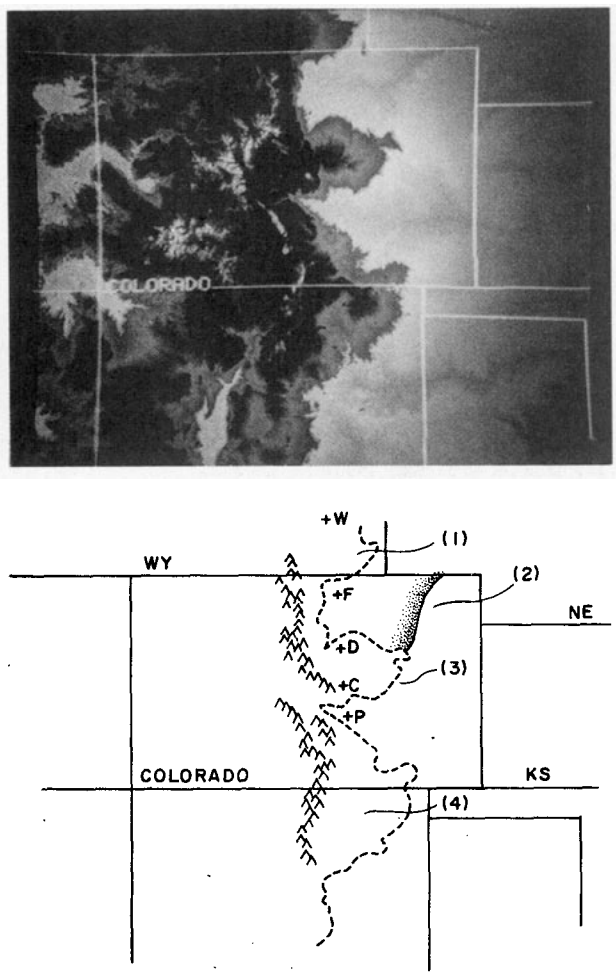

FIG. 1. (a) Terrain mapping of Colorado and surrounding vicinity. The brightest regions in central CO are the high ranges of the Rocky Mountains (elevations range from about 3000 to 4000 m). The elevations in the eastern portion of the figure (on the right) range from about 600 to about 1500 m (at the ridgelines named in panel b). (b) Diagram corresponding to the terrain photo in panel a. Feature 1 is the Cheyenne Ridge, 2 is called herein the Yuma extension, 3 is the Palmer Lake Divide, and 4 is the Raton Mesa. F is Fort Collins; D, Denver; C, Colorado Springs; P, Pueblo; W, Wheatland, WY. Dashed line = 1500-m height contour.

rapidly evolving air-mass changes. The use of altimeter settings, in place of sea-level pressures, eliminates many of the problems associated with rapidly evolving systems. In addition, S87 describes an adjustment to altimeter settings which reduces the remaining problems caused by sloping terrain. Recently, Pielke and Cram (1987) and Danard (1989) have described alternatives to S87. Also, Doswell (1988), Davies-Jones (1988), and Cram and Pielke (1989) present detailed discussion of both the S87 and the Pielke and Cram techniques.

In this section, another technique (actually a modification of S87) will be briefly developed. This technique is designed to account approximately for the effects of sloping terrain, and to be simple enough to be applied to a local area using a personal computer. The discussion which follows is supplemented by more rigorous material in the Appendix.

In common with S87, the modified technique described herein is based on the surface pressure being reported in the form of an altimeter setting (ALT). Also in common with S87, we recognize that in areas with sloping terrain, when the atmosphere is much warmer or colder than standard, an analysis of ALT may amount to little more than an analysis of terrain elevation. Thus, like Sangster, we compute an adjusted altimeter setting (ADJALT) for each observation; the adjustment accounts for the errors introduced by virtual temperature deviations from the standard atmosphere. The form that our adjustment takes is

$$\text{ADJALT} = \text{ALT} - [S'(Z_p - Z')/(\Delta D/\Delta\text{ALT})]. \quad (1)$$

The factors which constitute the bracketed term (i.e., the adjustment to ALT) will be briefly discussed in the following few paragraphs. However, we will refer frequently to the Appendix, which gives a more detailed discussion of each factor.

In the above formulation, D is what is commonly referred to as the "D-value." It is the difference at the time of the observation between the actual height of the observation site Z, and the pressure height in the standard atmosphere Z_p. The factor in the denominator ($\Delta D/\Delta$ALT) simply converts D-values to ALT values (i.e., pressure units). This factor is approximately a constant, and is discussed in detail in the Appendix (see Eqs. A9–10).

The level Z' is a constant baseline pressure height. It serves as a reference level which allows for comparison of stations at different elevations. The quantity $(Z_p - Z')$ is the vertical distance between a particular observation and this arbitrarily chosen pressure height. Z' should be chosen as close as possible to the average pressure height in the area of interest. This choice minimizes the overall amount of adjustment in the mesoscale area of most concern.

The final factor S' is related to Bellamy's (1945) specific virtual temperature anomaly,

$$S^* = (T_v - T_p)/T_p. \quad (2)$$

The specific virtual temperature anomaly measures the fractional deviation of the temperature at a station from that of a standard atmosphere (T_v is the virtual temperature and T_p is the standard as defined in the Appendix). Here, S' is the integrated effect of specific virtual temperature anomalies in a reference atmosphere that is calculated under various approximations and assumptions to S^* (see Appendix for details). One typical approximation is that S^* is only a function of height (Z_p). Since within a large mesoscale air-mass temperature typically varies much more rapidly vertically than horizontally, this is reasonable. In this in-

stance, S' specifies how rapidly the altimeter setting changes with height. It is this change that forces one to adjust the altimeter setting.

In this section we present a few examples which illustrate the relationship between S' and S^*. The examples are presented in order of increasing complexity, and consider three neighboring surface stations, designated herein as AAA, BBB, and CCC.

Case 1: All three stations are at the same elevation and, therefore, at approximately the same pressure height.

No altimeter adjustment is required.

Case 2: Two of the stations AAA and BBB are at different Z_p and also have different values of S^* (in this example, 0.05 and 0.03, respectively).

Bearing in mind that the ultimate goal is to obtain the surface *horizontal* gradient of ALT, consider one component of this gradient along a line connecting the two stations (Fig. 2a). A representative average value for this component is given by the sum of the changes in ALT along only the horizontal branches of the dashed path in Fig. 2a. The changes along the vertical branches need to be subtracted from the observed difference in ALT between AAA and BBB. These vertical changes depend on the surface values of S^*, which vary. However a quick and reasonable solution is to average S^* between AAA and BBB. Thus $S' = 0.04$ could be applied to the ALT at BBB and used to adjust it up to AAA's level ($Z' = 2000$ m). Alternatively, AAA could be adjusted down to BBB's level ($Z' = 1000$ m) also using $S' = 0.04$. In either case the *gradient* of ADJALT would be the same. If Z' was at an intermediate level then the appropriate values for S' would change. The gradient of ADJALT would remain the same.

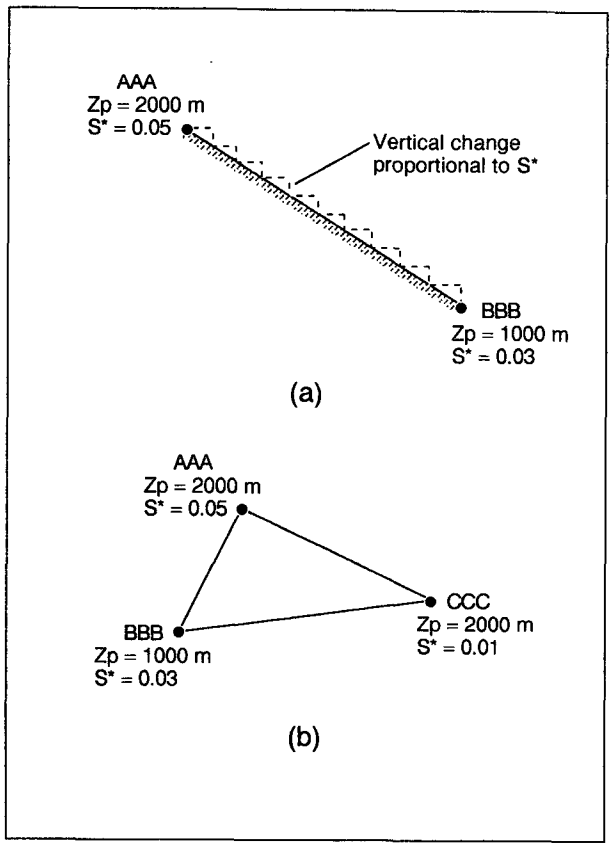

FIG. 2. Observations of Z_p and S^* plotted at hypothetical stations: (a) a vertical cross section illustrating adjustment process along earth's surface; and (b) a horizontal plot showing relative location of the three stations discussed in section 2, example case 3.

Case 3: The third station, CCC, is at the same pressure height (2000 m) as station AAA. The observed S^* at CCC (0.01) is different than at AAA (0.05).

This situation is illustrated in Fig. 2b. Stations AAA and BBB are the same as in the previous case, and so BBB could be adjusted up to AAA's level (2000 m) using $S' = 0.04$. However based on CCC's observation, BBB should be adjusted up to 2000 m using instead $S' = 0.02$. This change would improve the BBB–CCC portion of the ADJALT analysis but introduce an error in the BBB–AAA portion. There is no single correct solution; some compromise is required. This is the problem with actual observations; S^* generally depends not only on Z_p but also varies between stations with the same Z_p. Thus it is impossible to eliminate entirely the pressure-analysis error due to elevation differences. An analysis with many stations requires some compromise.

In summary, ADJALTs are obtained using an appropriate value for S' at each station. This value depends not only on the S^* observed at that station but also on the observations at surrounding stations. Much of the error introduced using sea-level-pressure analyses can be eliminated by using ADJALT analyses. For the remaining unavoidable error, our philosophy for a mesoscale analysis is to shift the error as much as possible away from the area of interest. Which area is of most interest is a subjective decision, dependent on the particular situation. Following an overview of the severe weather case in section 3, the ADJALT technique is applied to that specific area of interest.

3. Application to a case study

A major outbreak of severe weather occurred on 2 August 1986 along the Front Range of the Rocky Mountains. (See Fig. 1 for locations of topographic and geographic features.) The outbreak was somewhat unusual in that the severe storms remained close to the mountains rather than moving rapidly into the sparsely populated areas well to the east. There were numerous reports of 2.0–7.5 cm (0.75–3.0 in.) hail, with extensive damage in many Front Range cities (Storm Data 1986). Total damage estimates range as high as $200 million. In rural areas, thousands of birds

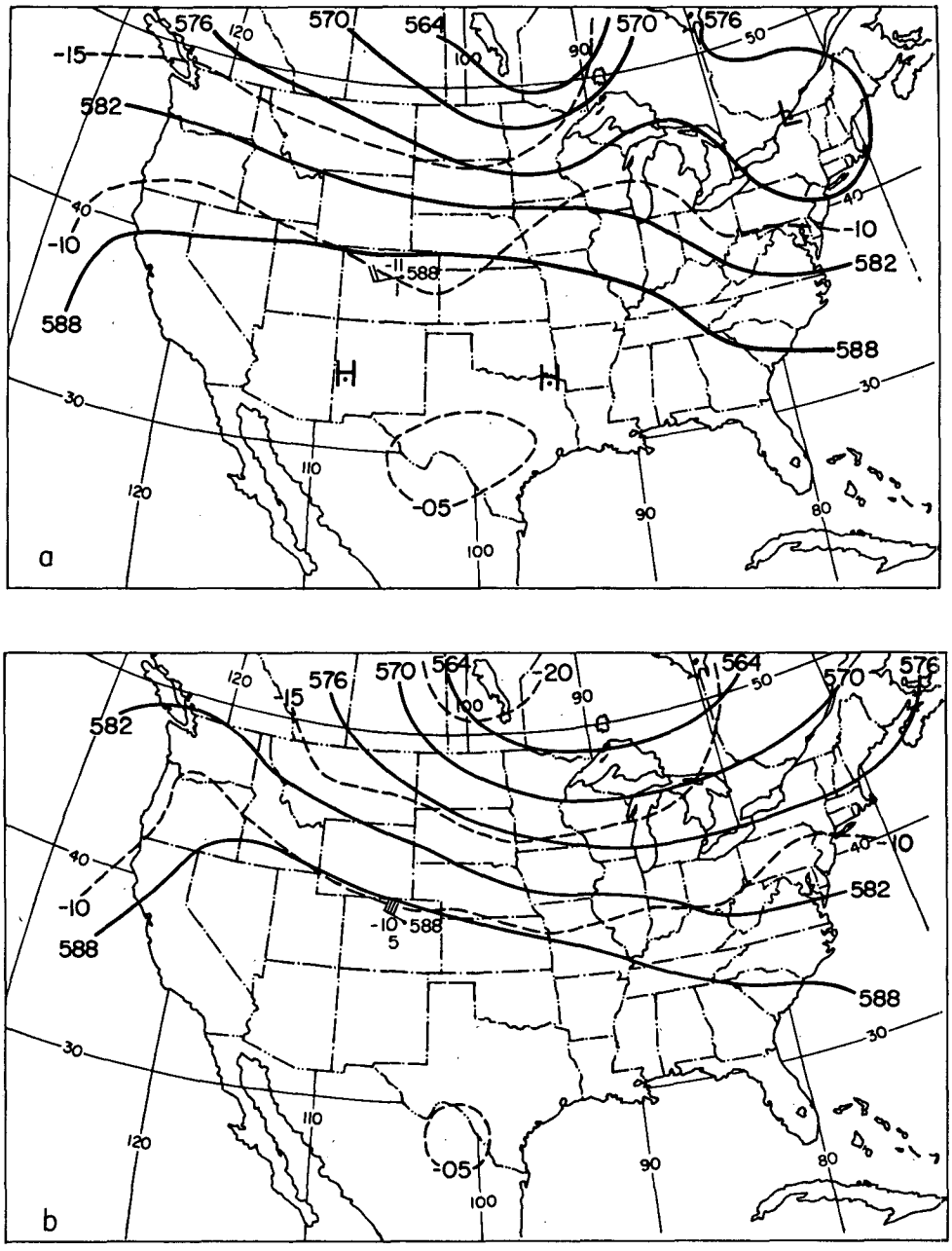

FIG. 3. 500 mb analysis from 1200 UTC: (a) 31 July 1986, and (b) 1 August 1986 [heights are in decameters (solid), temperatures in °C (dashed)]; also, abbreviated surface analysis from 1200 UTC (c) 31 July 1986, and (d) 1 August 1986. Symbols are conventional.

and hundreds of small farm animals were killed or injured, and crop damage totaled well over $100 million.

a. Synoptic pattern

A weak Pacific front entered the northwest United States on the late afternoon of 28 July 1986. Over the next few days the front propagated slowly eastward and southeastward, passing through eastern Colorado (CO) during the morning of 30 July. By 1200 UTC 1 August, the northern portion of the front had pushed into the Ohio valley, while the southern end had become quasi-stationary in the vicinity of the Kansas (KS)–Oklahoma (OK) border (Fig. 3c, d). Upper-air analyses (Fig. 3a, b) also showed enhanced baroclinicity over Nebraska (NE), indicating large-scale dynamics potentially stronger than would normally be expected over the Central Plains in late July and early August.

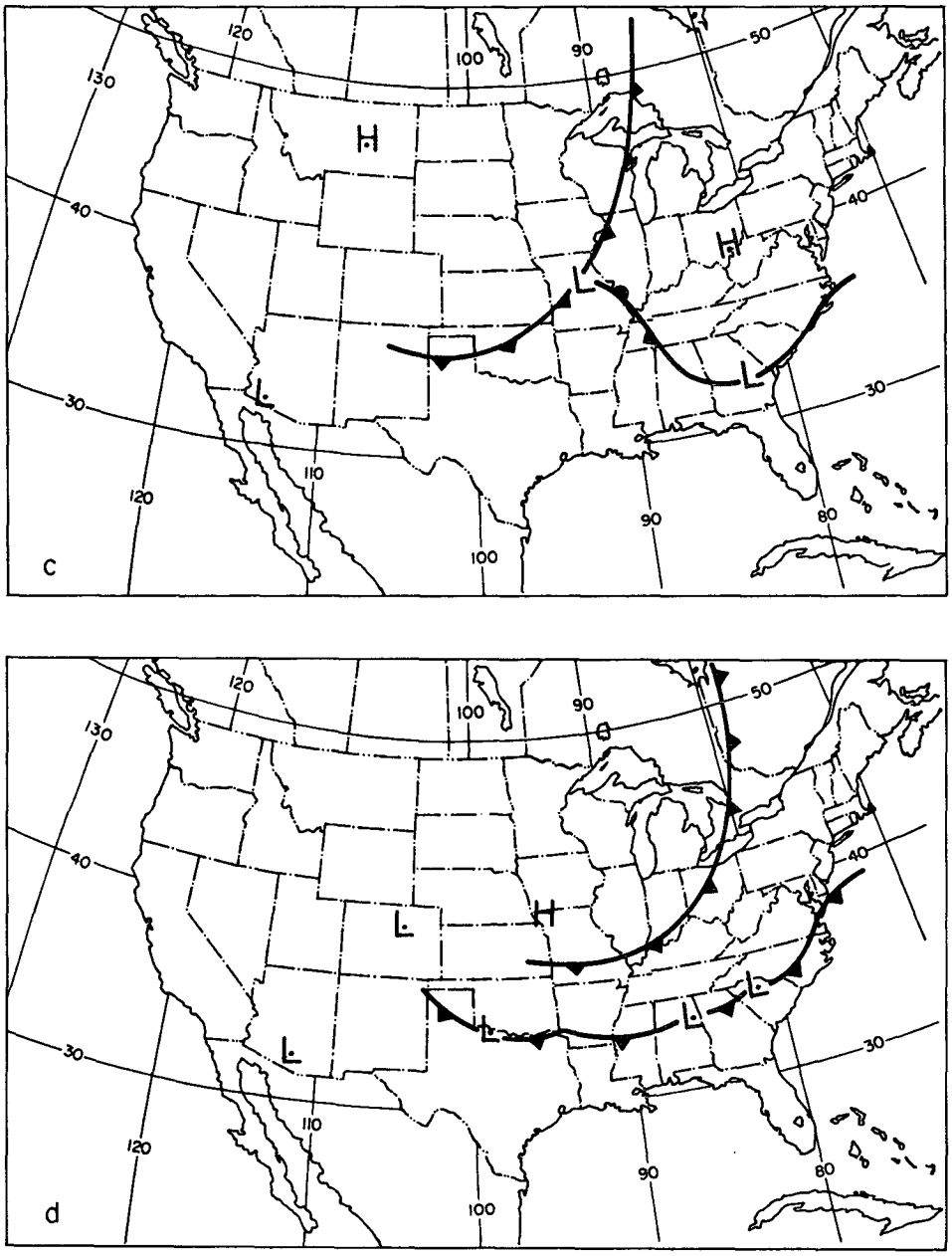

FIG. 3. (*Continued*)

Beginning on 31 July and continuing through 2 August, the synoptic situation evolved into a pattern favorable for severe thunderstorms over the High Plains (Doswell 1980). The passage of the cool front left eastern portions of CO and Wyoming (WY) in low-level, easterly, upslope flow. Such a pattern tends to advect moist air westward to the Front Range of the Rockies. Indeed, dewpoints in southeast WY and northeast CO had exceeded 10°C (50°F) by 31 July. During a 3-day period, this general synoptic pattern brought severe weather to eastern WY, eastern CO, western NE and western South Dakota (SD).

b. The u-shaped area

One of the interesting aspects of this case was the way in which the outflow from a large nocturnal MCS in WY and NE moved into northeast CO during the morning of 1 August 1986. Specifically, this cooler, more moist air entered the region as a u-shaped wedge. The new air mass pushed westward to the Front Range of the Rockies (where further progress was blocked), and southward to the Palmer Lake Divide. The western and southern edge of this cooler air was marked by small cumulus to the west, and an east-west line of

towering cumulus to the south in Fig. 4. The eastern edge spread eastward, eventually becoming blocked by a shallow, northeastward extension of the Palmer Lake Divide, henceforth referred to as the Yuma extension (Fig. 1). The ability of this shallow terrain feature to block the mesoscale cold surge will be discussed later.

The u-shaped area has been of mild interest to Colorado forecasters for several years. Summertime convection is common over the Palmer Lake Divide, and over the much higher terrain to the west. However, sometimes convection forms to the east along the Yuma extension as well. When this occurs, the perimeter of the area takes on a u-shaped appearance as illustrated in Fig. 5. The Yuma extension is very shallow, and therefore much less effective than the Front Range and the Palmer Lake Divide, both in forcing upslope flow, and in blocking air masses. Nevertheless, it is a favored location for the eastern boundary of such air masses within the u-shaped area. One of the most significant cases in which this area played a role was the unusual severe weather outbreak of 15 October 1980, discussed by Weaver and Brown (1982). In that case, moist, potentially unstable, low-level air trapped within the u-shaped area was credited with being an important contributor to the occurrence of an out-of-season tornado in Boulder, CO, and of large hail and heavy rains in other parts of northeast CO.

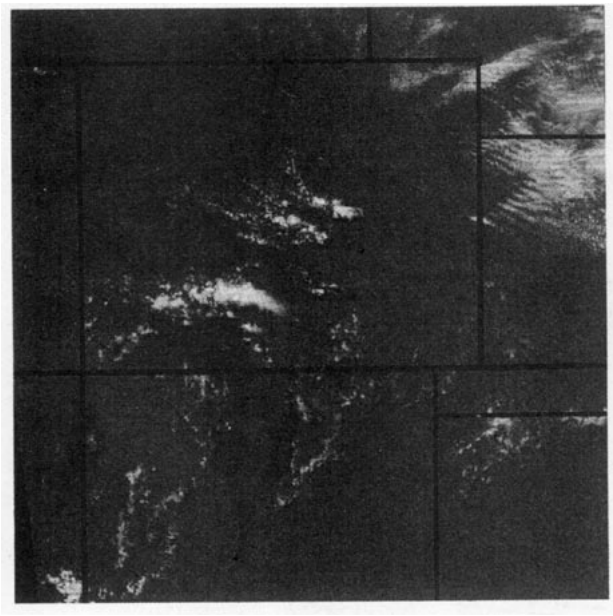

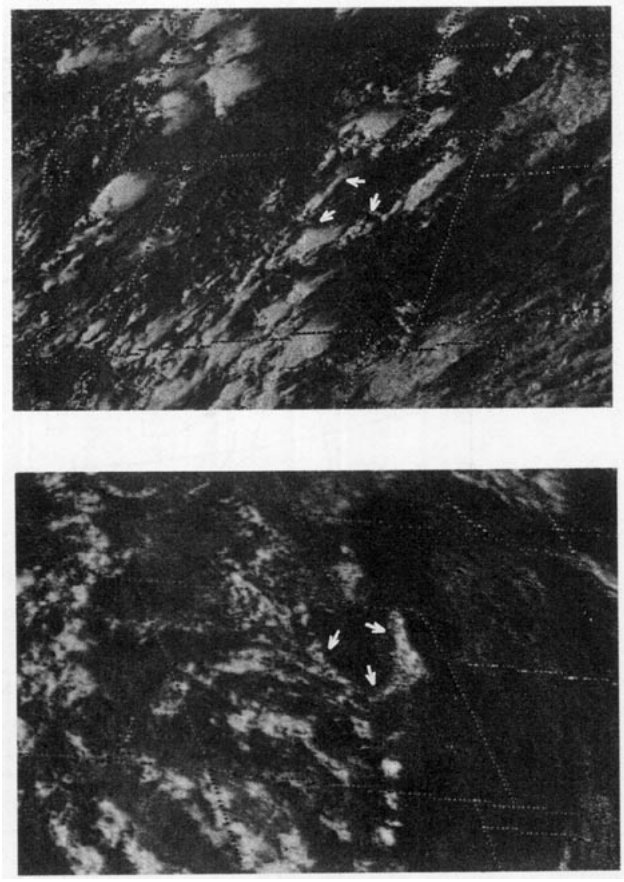

FIG. 5. The VIS satellite images from (a) 1945 UTC 10 July 1981, and (b) 2230 UTC 17 August 1981 illustrating the development of convective clouds around the perimeter of the u-shaped area (see text) in northeastern CO.

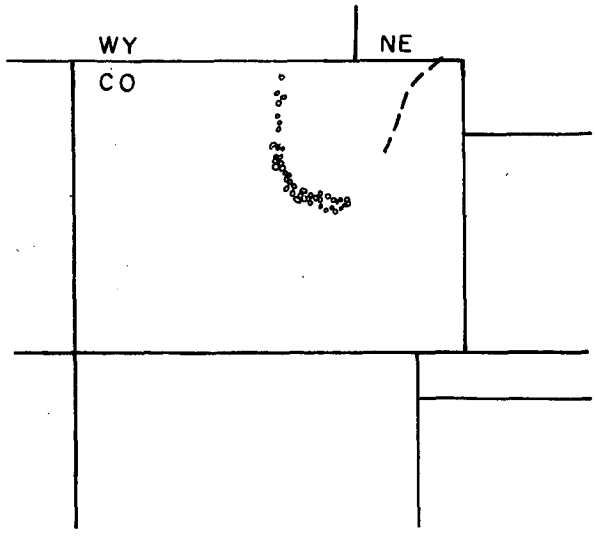

FIG. 4. (a) Visual wavelength (VIS) satellite photo from 1800 UTC 1 August 1986, centered over Colorado; (b) schematic of part of panel a, illustrating the western and southern cloud lines referred to in text (scalloped) and approximate location of Yuma extension (dashed).

c. *Mesoscale overview*

By the late evening of 31 July, the mesoscale situation in northeast Colorado was already beginning to evolve into what would culminate in the severe weather

of 2 August. A few small thunderstorms had formed along the Yuma extension during the afternoon, but they produced only rain and small hail. Then at approximately 0000 UTC 1 August, a thunderstorm formed on the Cheyenne Ridge, near Wheatland, WY (Fig. 1). Over the next 4 h, this storm moved into and across extreme northeast Colorado, producing 3.8 cm (1.5 in.) diameter hail along much of its path. The storm itself was very large and a trailing outflow could be seen quite clearly on infrared-satellite imagery (Fig. 6). Cooler air from this storm slipped into the u-shaped area and remained relatively cooler for several hours.

At 0500 UTC 1 August, a thunderstorm formed in extreme northeast WY on the leading edge of a minor-shortwave trough. The single storm grew gradually into a large MCS (Fig. 7) as it moved slowly southeastward. Animated satellite imagery near sunrise on 1 August indicated that the western edge of the cool surface outflow from the MCS pushed into the u-shaped area to reinforce the (by now) modified outflow from 0000 UTC. Conventional analyses did not clearly indicate this intrusion (Fig. 8), although there is perhaps a slight

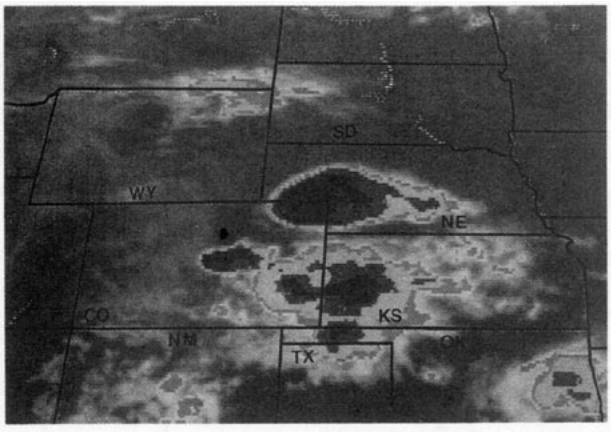

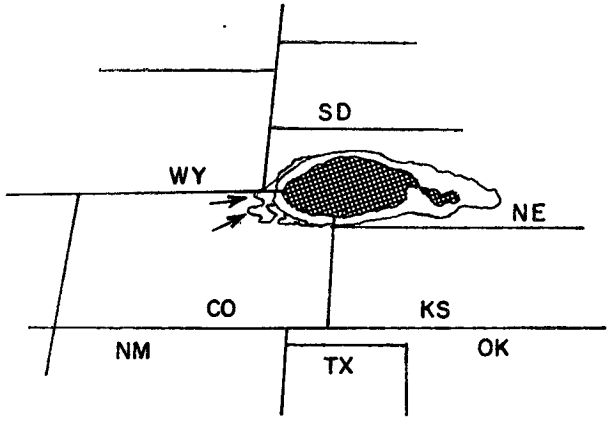

FIG. 6. (a) Infrared wavelength (IR) satellite photo from 0400 UTC 1 August 1986 illustrating the large severe thunderstorm complex over northeastern CO. (b) Schematic of storm referred to in text. Arrows show warmer (lower) clouds associated with outflow.

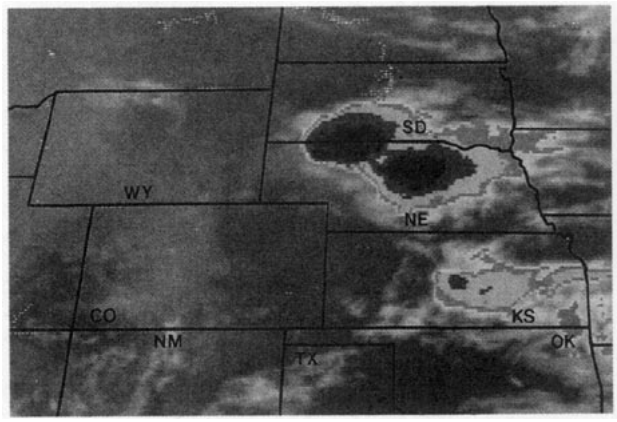

FIG. 7. IR satellite photo from 1301 UTC 1 August 1986 illustrating the large MCS over south-eastern SD and north-central NE.

hint of its presence in the analysis of equivalent-potential temperature (Fig. 8d) as well as in wind shifts recorded at individual stations. The ADJALT analyses, however, provided a clear signal of the development of this mesoscale air mass.

d. Adjusted altimeter analyses

The first step in constructing an ADJALT analysis is to select Z'. A natural choice for the Front Range hailstorm case was $Z' = 1600$ m. (Note the location of major Front Range cities relative to the 1500-m terrain height contour in Fig. 1.) The second step is to determine appropriate values for S'. This determination is aided by plotting observations of S^* vs Z_p. Such a plot is shown in Fig. 9 for 1800 UTC 1 August. At a constant elevation, S^* tends to increase to the south, and so there will be some unavoidable error in the ADJALT analysis. However, S^* also tends to increase with height. This increase with height can be adjusted for by assuming an approximate S^*. The sloping line in Fig. 9 indicates an approximate S^*, chosen subjectively to best fit the observations within the MCS outflow in the northern part of the analysis area. This line is given by

$$S^* = 0.073 + (0.023\ \text{km}^{-1})(Z_p - 1.6\ \text{km}). \quad (3)$$

As shown in the Appendix, an equation for S^* allows one to determine an equation for the adjustment parameter

$$S' = 0.073 + (0.0165\ \text{km}^{-1})(Z_p - 1.6\ \text{km}). \quad (4)$$

In other words, the rate of change of S' is half the rate of change of S^*. These values of S' are then applied at each station regardless of the observed S^*. The factor $(\Delta D/\Delta \text{ALT})$ in Eq. (1) is approximated using Eq. (A10) from the Appendix. A subjective analysis of the resulting ADJALTs is shown in Fig. 10c (M1 indicates Method 1). For comparison, the conventional synoptic analysis of sea-level pressure (Fig. 10a) and an analysis

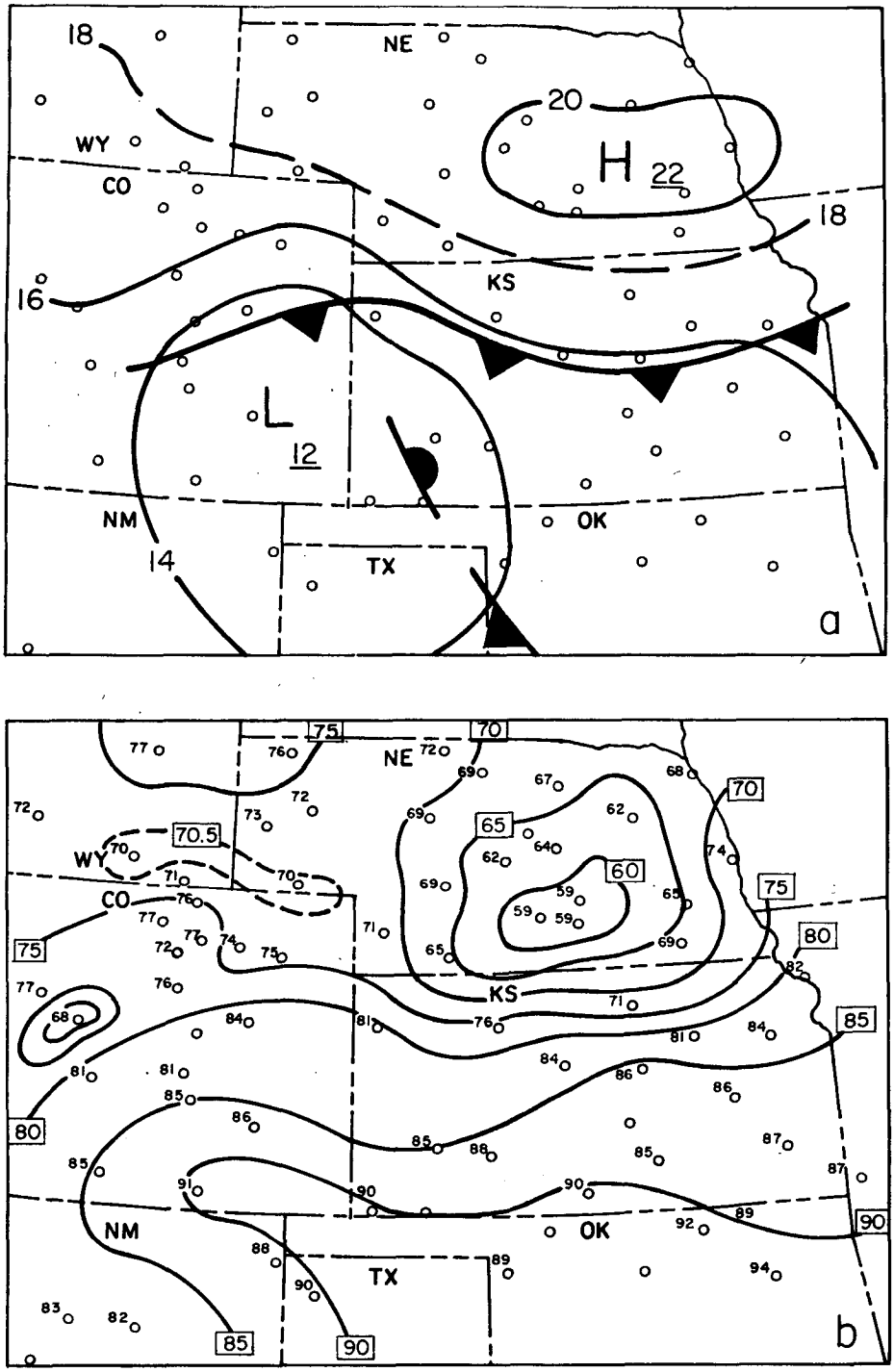

FIG. 8. Analyses of various surface variables for 1800 UTC 1 August 1986. Parameters include (a) sea-level pressure with surface fronts (leading 10 omitted on mb pressure values), (b) temperature in degrees F, (c) dewpoint in degrees F, and (d) equivalent potential temperature in degrees K. Wind barbs are conventional.

of raw altimeter settings (Fig. 10b) are also shown. Raw altimeter settings increase very rapidly as the terrain height increases to the west. The M1 adjustment has eliminated most of this increase, leaving what should be a better indication of the actual horizontal pressure gradient. This is particularly true across

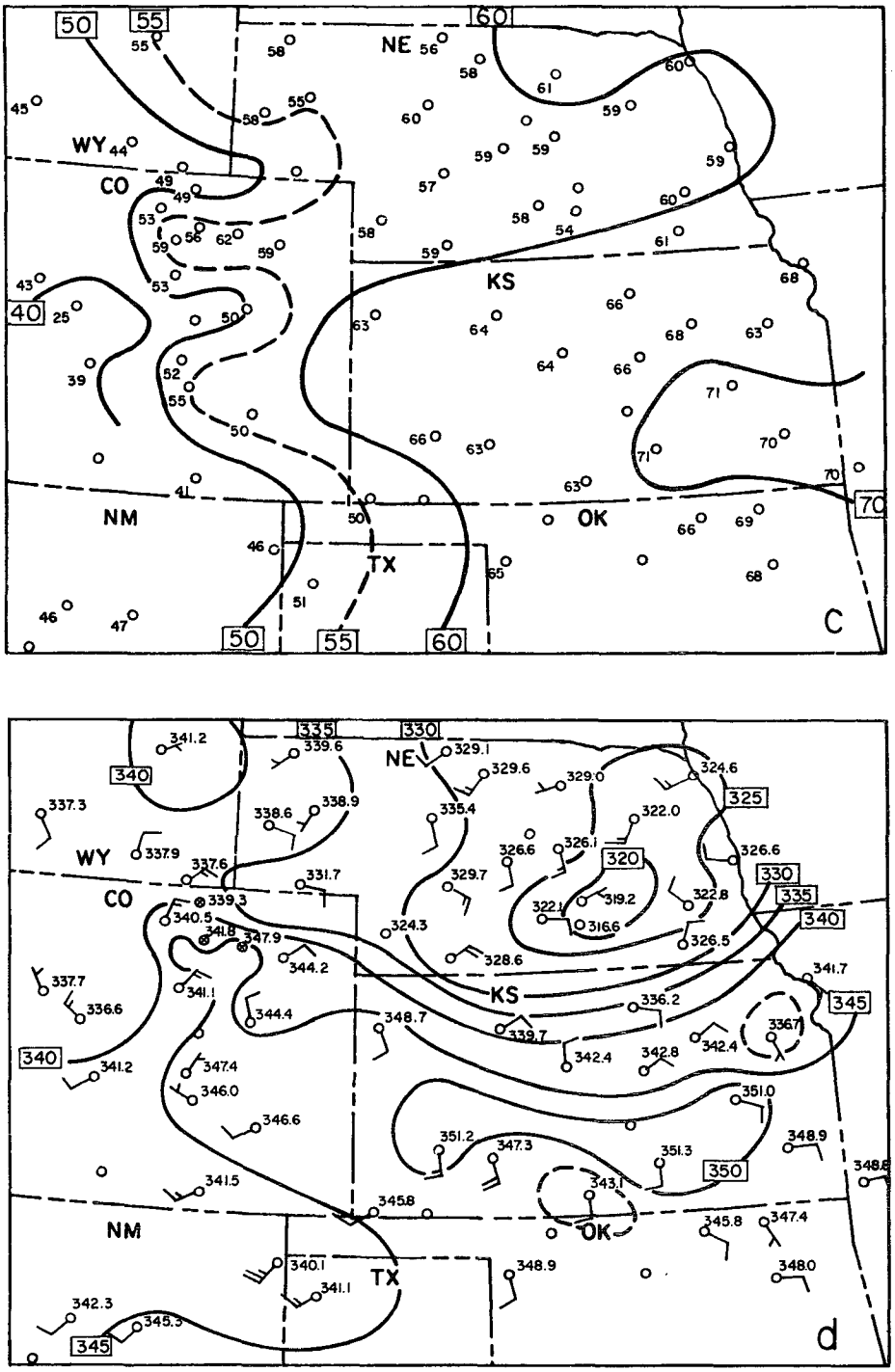

FIG. 8. (*Continued*)

northeast CO and northern KS, where the temperature deviation used for adjustment closely fits the observations (Fig. 9). Notice that over high terrain the analysis of sea-level pressure erroneously indicates a stronger easterly component of the surface geostrophic wind near the analyzed cold front—a consequence of a westerly thermal wind within the hypothetical layer of air between sea level and the surface. But even with its flaws, an analysis of sea-level pressure over sloping terrain is clearly preferable to an analysis of raw altimeter

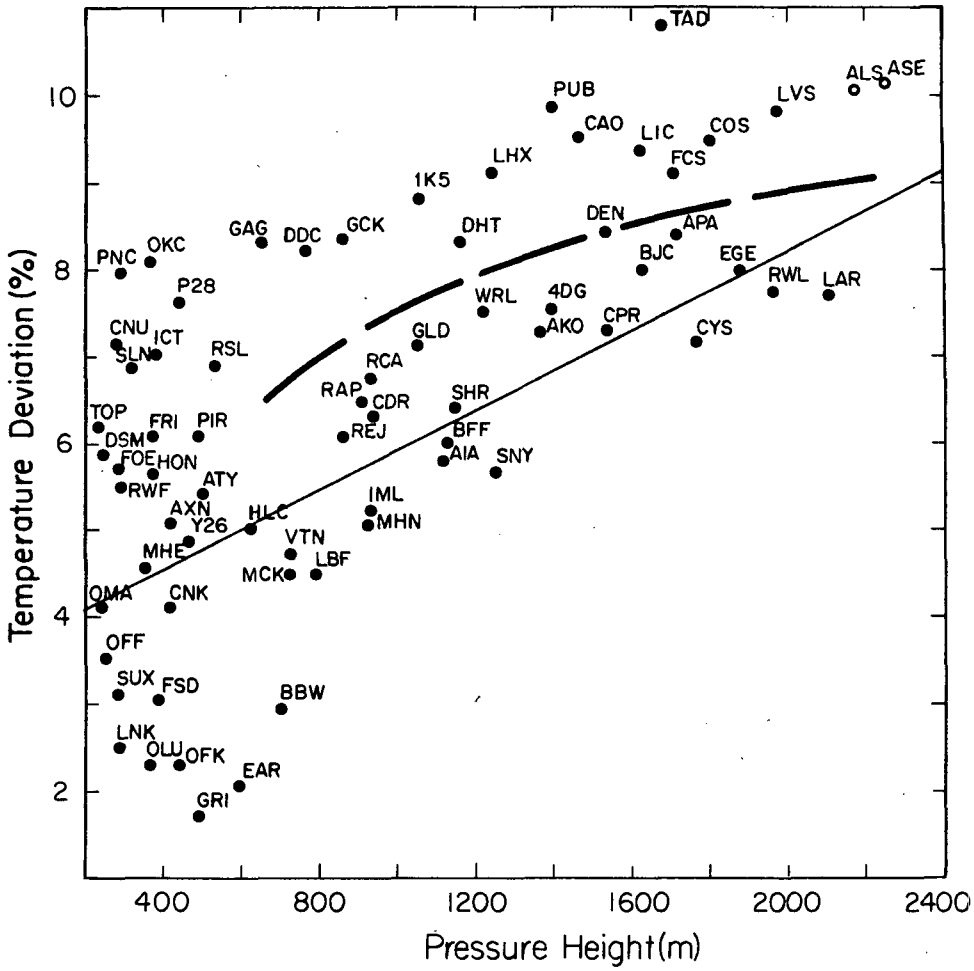

FIG. 9. Surface observing sites (three-letter identification) plotted vs pressure height (Z_p; horizontal axis) and temperature deviation (S^*; vertical axis). Dashed curve separates warm air over the southern portion of the analysis area from the cooler, mesoscale outflow air to the north. Solid sloping line is the approximate S^* used for the adjustment in method 1, which was optimized for the cooler air mass (below the dashed curve).

settings whenever temperatures deviate significantly from their standard atmosphere values.

The M1 adjustment yields a horizontal pressure gradient that is more consistent with the evolution of the mesoscale air mass within northeast CO (as suggested by satellite imagery). However, after adjustment, altimeter settings continue to increase too rapidly with elevation in the warmer air along the KS–OK border and across southern CO (Fig. 9). This introduces an error in the analyzed southerly component of the geostrophic wind. The error depends on the terrain slope and is independent of Z'. A separate analysis optimized to correct this error in the warmer air would introduce new errors in the colder air.

To address this problem a further refinement, called herein method 2 or M2 was introduced. In this method, S' is recalculated for each station. This is done by taking the average of the 1600 m S^* used in M1 (0.073) and the observed S^* at each station. The reasoning behind this second method is based on Fig. 2b and is discussed further in the Appendix. The effect of the change from M1 to M2 is to improve the analysis (Fig. 10d) at elevations that are close to Z', and to degrade the analysis over much higher or much lower elevations. For example, the mesohigh over southeast NE, where the terrain slope is relatively small, was well analyzed with both the raw altimeter settings (Fig. 10b) and with M1 (Fig. 10c). This area is poorly analyzed with M2 (Fig. 10d), but there is a compensating improvement in the analysis of the southerly geostrophic flow within the warm air over the higher plains. Notice the analysis of the old frontal trough near the Texas (TX) and Oklahoma (OK) panhandles. The pressure gradient to the northeast of the trough agrees with the moderate southerly winds observed there. (The raw altimeter setting analysis indicates a *northerly* geostrophic wind

in the same area.) Closer to the mesoscale ridge in northeast CO, the M1 and M2 analyses are virtually identical. Since this paper will concentrate on developments over the western half of the area, only method 2 will be shown in the remaining analyses.

4. Detailed mesoscale synopsis

a. Development on 1 August

By midmorning of 1 August the ADJALT analysis showed a rather broad, diffuse area of low pressure dominating most of eastern CO (Fig. 11). A weak pressure trough extended eastward from the low across KS. However, this relatively bland pattern was being quickly replaced by rain-cooled air, and a complex pressure field associated with the large MCS discussed earlier (section 3c).

Over the next few hours, the rain-cooled air moved rapidly across the plains of southern NE and northern KS. In northeast CO, however, the situation was complicated by higher terrain, and by a preexisting temperature inversion. Along with the normal nocturnal cooling, this inversion was due, at least in part, to severe thunderstorms that occurred late the previous evening (refer section 3c). The "trapped" air developed into a significant mesoscale cold surge, which nosed rapidly southward (Figs. 4 and 10d), and eventually worked its way eastward some 200 km from the Front Range. The progression of this surge was followed using ADJALT analyses, and the satellite imagery (cloud development ahead of the boundary, lack of cloudiness behind it).

The diversion of the cold air toward the south (air that initially entered CO from the east-northeast) was likely a result of damming (Richwien 1980) by the high terrain of the Rocky mountains. In the analyses of ADJALT, the tight spacing of the isobars along the Front Range is the direct result of this damming effect. The development appears to be analogous to the alongshore surges of cold air documented by Mass and Albright (1987). In theory, the width of the topographically trapped cold surge depends on the depth of the cold air (approximately 1.9 km; see plot of Denver radiosonde, Fig. 12) and on the magnitude of the temperature inversion (approximately 5 K). Although the underlying Front Range topography is more complex than the sea surface used in the calculations by Mass and Albright, the theoretical width of the cold surge turns out to be 180 km, which is roughly in agreement with the eastward extent of the 1 August mesoscale cold surge. Coincidentally, this places the eastern edge near the Yuma extension. Presumably the cold air is very shallow at this point, thus providing the physical mechanism whereby in this and similar cases the Yuma extension could provide a block preventing further eastward movement of the cold air mass. Whether the Yuma extension plays a primary or a secondary role in determining the eastward extent of cold surges is a question that requires further study.

Late in the day the mesoscale cold surge slowed its southward progress as it encountered the Palmer Lake Divide. With strong daytime heating, it is difficult for a cold surge to maintain its gravity-current characteristics even over flat terrain (Garratt and Physick 1987). Although the cold air mass was nearly 2 km deep at its western edge, the impact of the heating would be magnified as the cold air tried to squeeze across the Palmer Divide. Of additional importance, diurnal heating over the high terrain to the west would tend to reduce the damming effect. Late in the afternoon there was evidence (windshifts, temperature falls, and minor pressure rises) that the cold air was able to move westward up to several mountain mesonet stations.

Although the cold surge stalled for several hours at the Palmer Lake Divide, by late afternoon (Fig. 13, 2300 UTC), it finally did spill across this east–west terrain boundary. Throughout the evening, the southern edge of the cold pool continued to play a role in forcing new convection in the Colorado Springs–Pueblo area.

b. Development on 2 August

Analysis of ADJALT throughout the night continued to show the effects of the MCS-induced pressure ridge. It is recognized that one must use caution when interpreting nocturnal pressure analyses, since such analyses are sensitive to surface temperature (Doswell 1988) and may reflect conditions within only a thin layer near the ground. Nevertheless, the amount of adjustment within northeast Colorado is small, and an analysis near dawn (Fig. 14) continued to show the mesoridge basically intact. Later analyses (e.g., 1600 UTC, Fig. 15), when warmer daytime temperature were reestablished, also carry the feature in a consistent manner. Figure 16 illustrates its persistence by presenting a 24-h average of the ADJALTs. While the averaging tends to obscure the transient features over most of the analysis area, the structure of the mesoridge in northeast CO is retained. The small dots plotted on the analysis constitute the 37 reports of large damaging hail which occurred later that day. It is interesting to note that 35 out of the 37 events occurred between the Front Range and the central axis of the MCS-induced mesoridge.

5. Concluding remarks and discussion

The 2 August 1986 case contains a large number of interesting and insightful aspects. Some of these have been addressed in detail in this paper, others only touched upon, and some were not even mentioned due to space and time limitations. For example, it is interesting that the 1 August 1986 MCS lasted more than

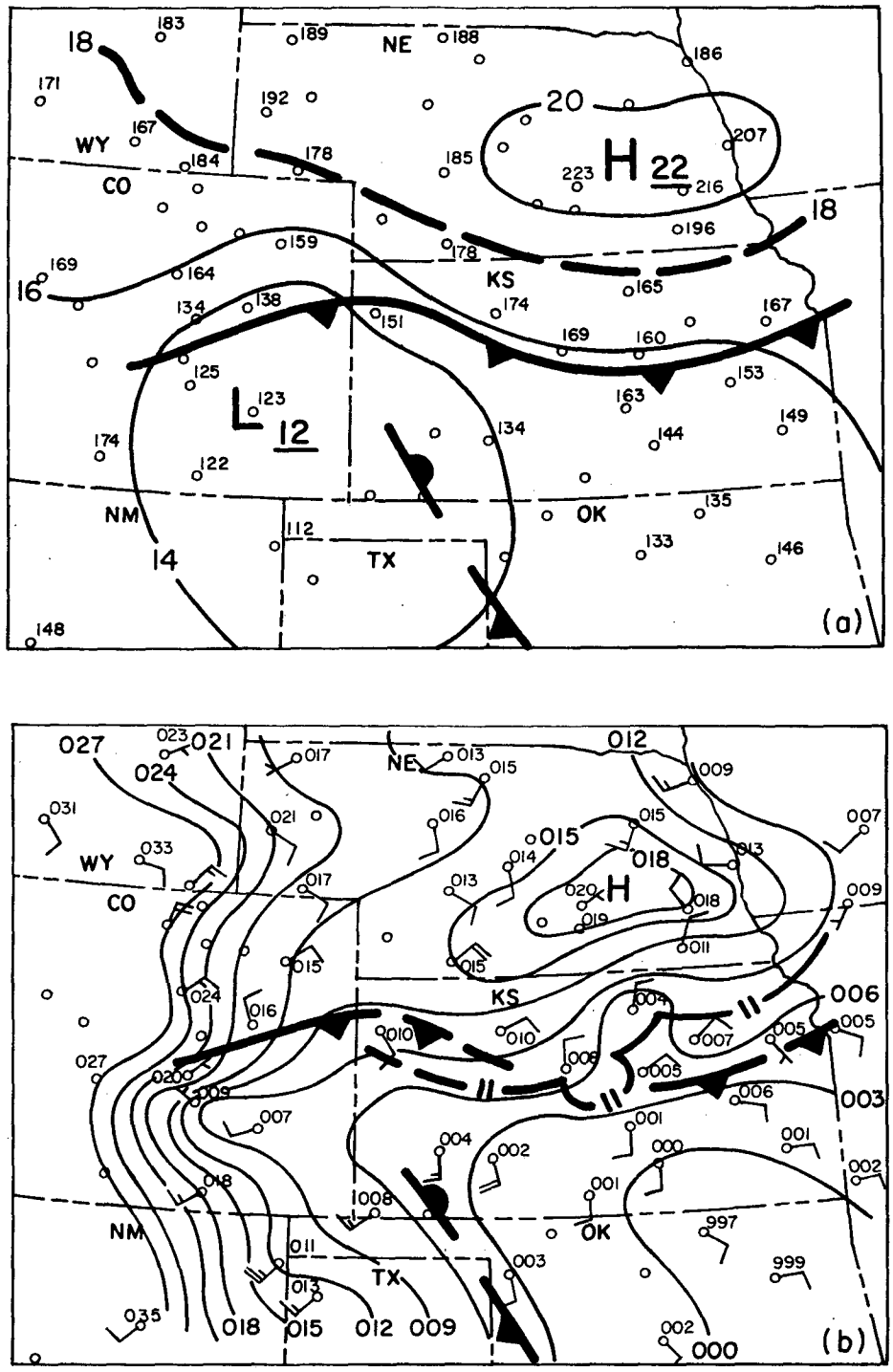

FIG. 10. Various pressure analyses for 1800 UTC 1 August 1986: (a) Standard NMC-based surface chart with sea-level pressure. Plotted pressure values are in millibars (leading two digits omitted), pressure contours as labeled, and surface features are in standard notation. (b) Altimeter settings (in inches Hg × 100 with leading digit omitted), pressure contours as labeled (contour interval of 0.03 in. Hg), surface features from NMC analysis plus outflow boundaries as located via satellite. (c) Altimeter settings adjusted using method 1 (see text), pressure contours as labeled (contour interval of 0.05 in. Hg), surface features as in panel b; however, an outflow boundary has been added along the southern edge of the mesoridge. (d) as in panel c, but altimeter settings adjusted using method 2 (see text).

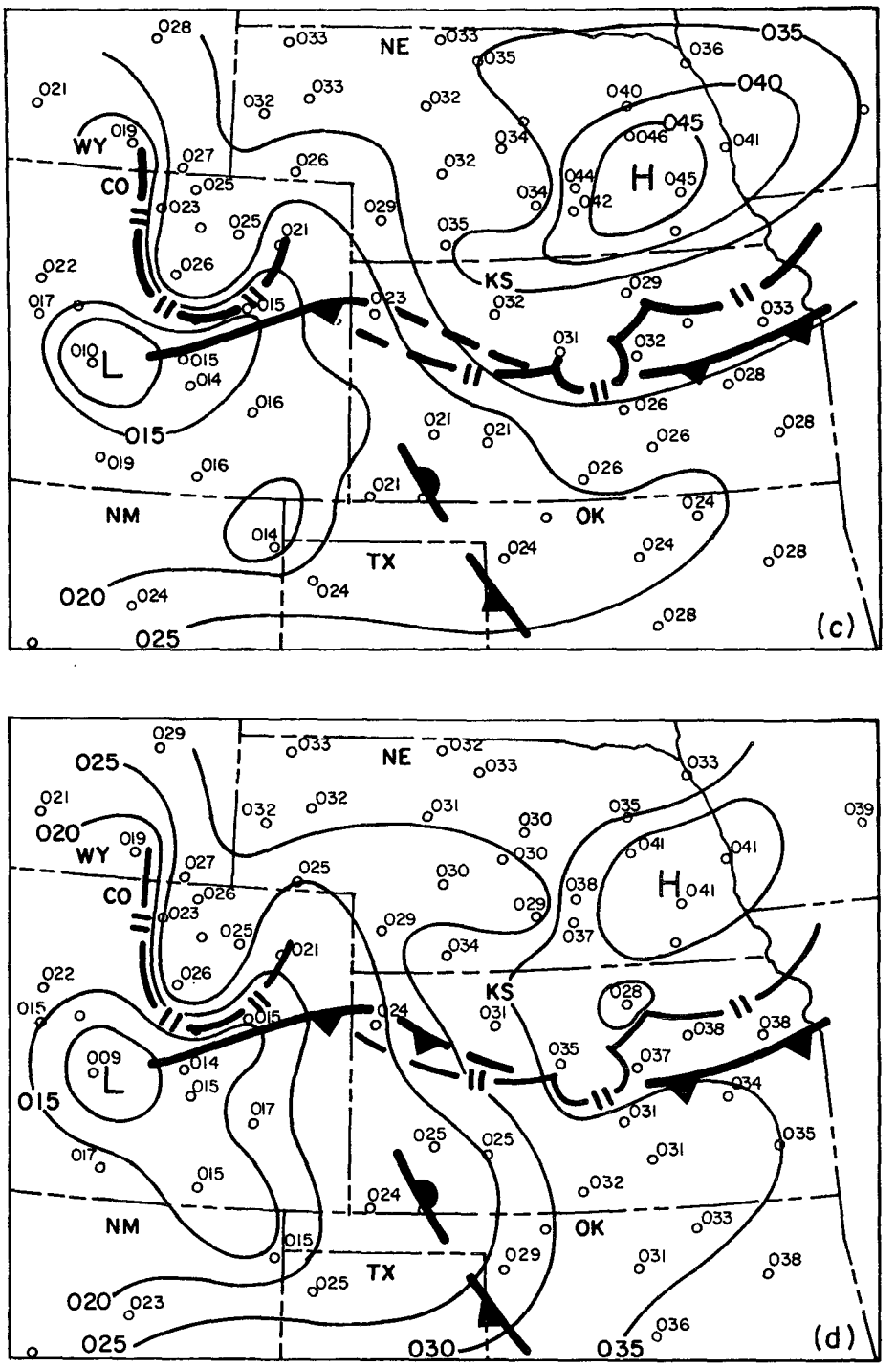

FIG. 10. (*Continued*)

24 hours, finally dissipating over the southeastern United States. Also, the intersection of the MCS with thunderstorm activity on the synoptic front in northeastern and north-central Oklahoma during the evening hours of 1 August could constitute a lengthy and worthwhile study.

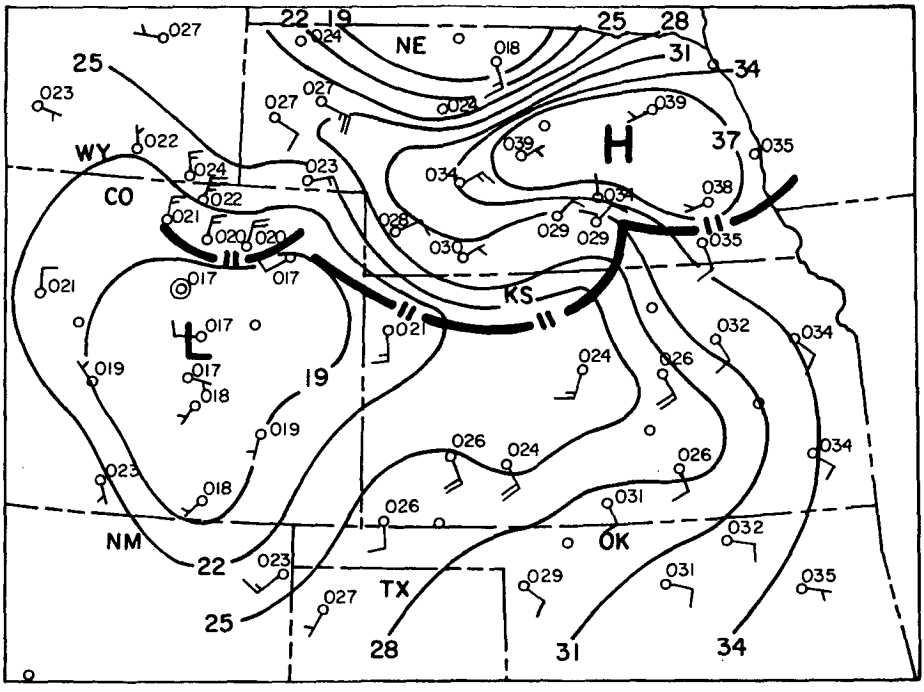

FIG. 11. Altimeter settings adjusted using method 2 (see text) for 1600 UTC 1 August 1986; pressure contours as labeled (contour interval of 0.03 in. Hg).

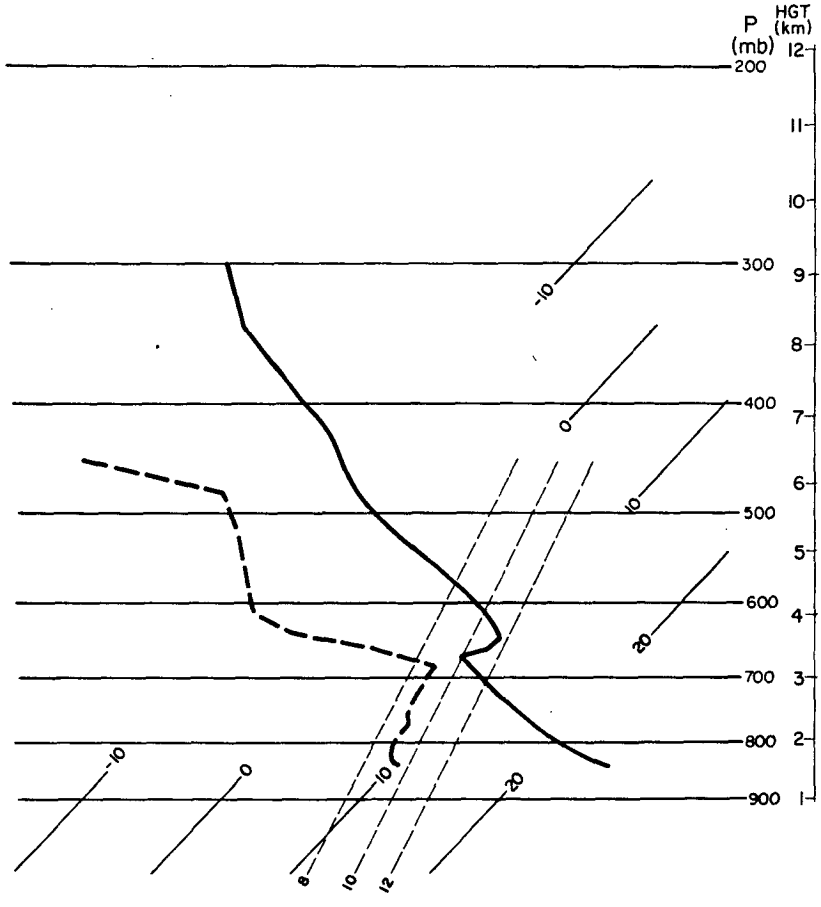

FIG. 12. Denver, CO, (DEN) radiosonde data for 0000 UTC 2 August 1986 plotted on a skew T-log P diagram. Solid line is temperature; dashed line, dewpoint temperature (both in degrees C).

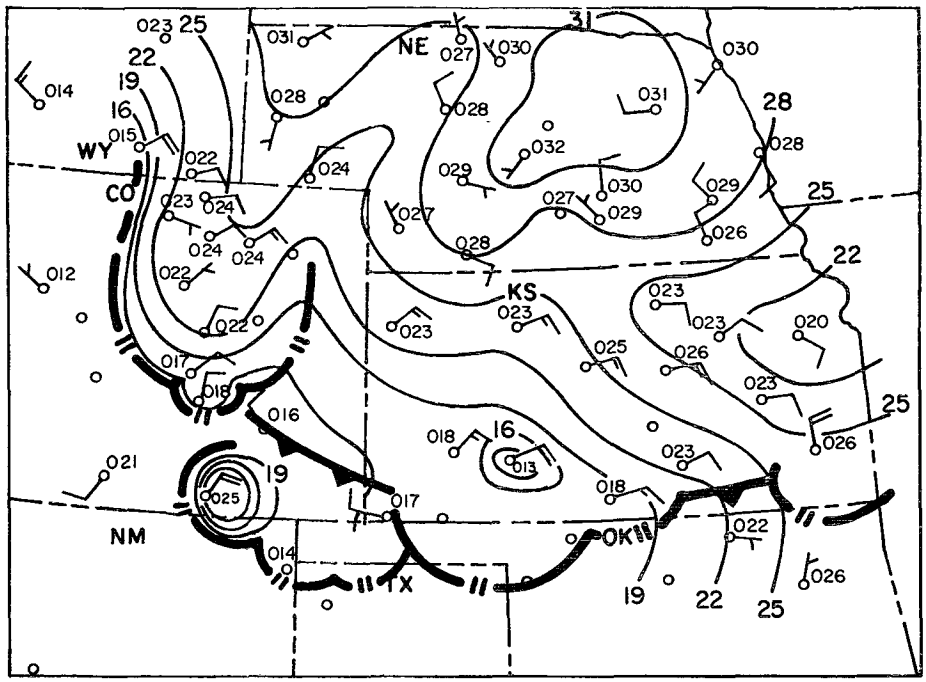

FIG. 13. As in Fig. 11, except for 2300 UTC 1 August 1986.

This study focuses on the residual effects of a mesoscale convective system. In a general sense, it is known that the effects of outflows from MCSs can be quite persistent (Weaver and Nelson 1982; McAnnelly and Cotton 1986). They are often fed cool, moist air by evaporating rainfall for hours after convective activity has ceased. In this case, the effects of the large, long-lived outflow were even more evident as the natural terrain barriers in CO kept the mesoscale cold surge compact and concentrated.

The major point of this paper concerns the importance of properly analyzing meteorological data. In many instances, features are observed on satellite imagery which conventional data, or data analyses, fail to isolate. In this case, the air mass in northeastern CO appeared significantly different from surrounding areas (on both 1 and 2 August) within satellite imagery, but conventional analyses failed to find this difference. By attempting to analyze a more realistic horizontal pressure gradient at the surface, a mesoscale ridge was identified which corroborated the information available from the *GOES* satellite. It is clear that the features seen within satellite imagery were important to the evolving situation, but were not substantiated by the more conventional analyses, and thus may have been passed over in the final synopsis by most forecasters. The technique presented herein is meant to, at least partially, overcome this difficulty in a manner that can be reasonably be accomplished in real time.

For the purpose of analyzing the pressure-gradient force at the surface, sea-level pressure is the "industry standard" (Doswell 1988). There are unavoidable errors over sloping terrain, but part of the problem with sea-level pressure can be avoided by accounting for the combined effects of temperature gradients and terrain. By eliminating the unnecessary error, and by focusing on a limited, mesoscale area, the analyses of the horizontal pressure gradient may be made to more closely represent the forces affecting that small area. It is true that such a mesoscale analysis, based on Sangster's (1987) technique, is sensitive to temperature (density) errors; but provided that the temperature observations are representative of the surrounding area, there is nothing in the ADJALT technique which prevents the error from being kept within the reporting-error limits (0.01 in. Hg).

A recurrent feature of summertime weather in eastern CO is the development of the daily upslope cycle (e.g., Toth and Johnson 1985). Upslope flow is a primary ingredient in the atmosphere for setting up the occurrence of severe thunderstorms on the High Plains (Doswell 1980). The upslope flow on 2 August 1986 was reinforced both by the synoptic, postfrontal gradients, and more importantly by flow responding to a persistent mesoscale ridge of high pressure in northeastern CO. It is likely that the enhanced upslope flow became even more vigorous in early afternoon through the mechanism of damming breakdown as discussed in section 4. We suggest that the result of this accelerated upslope flow was a deep layer of exceptionally

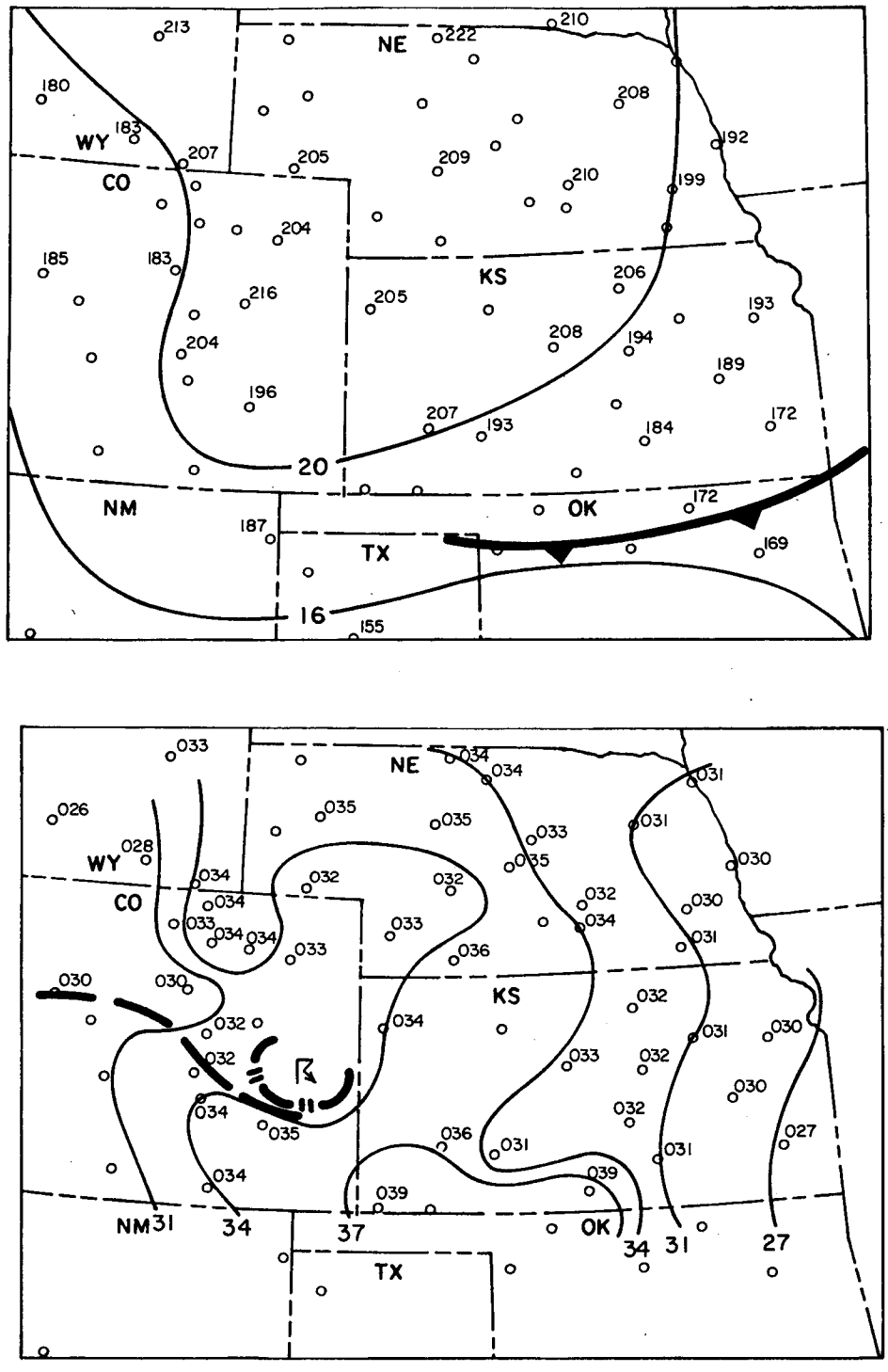

FIG. 14. (a) As in Fig. 11, except for 1200 UTC 2 August 1986; (b) as in Fig. 8a, except for NMC surface chart for 1200 UTC 2 August 1986.

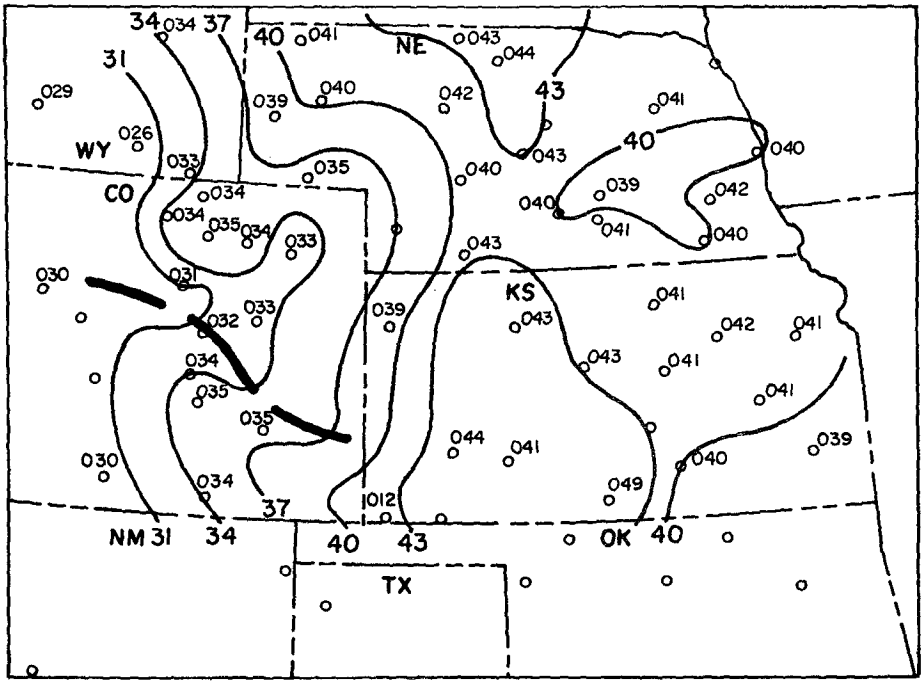

FIG. 15. As in Fig. 11, except for 1600 UTC 2 August 1986.

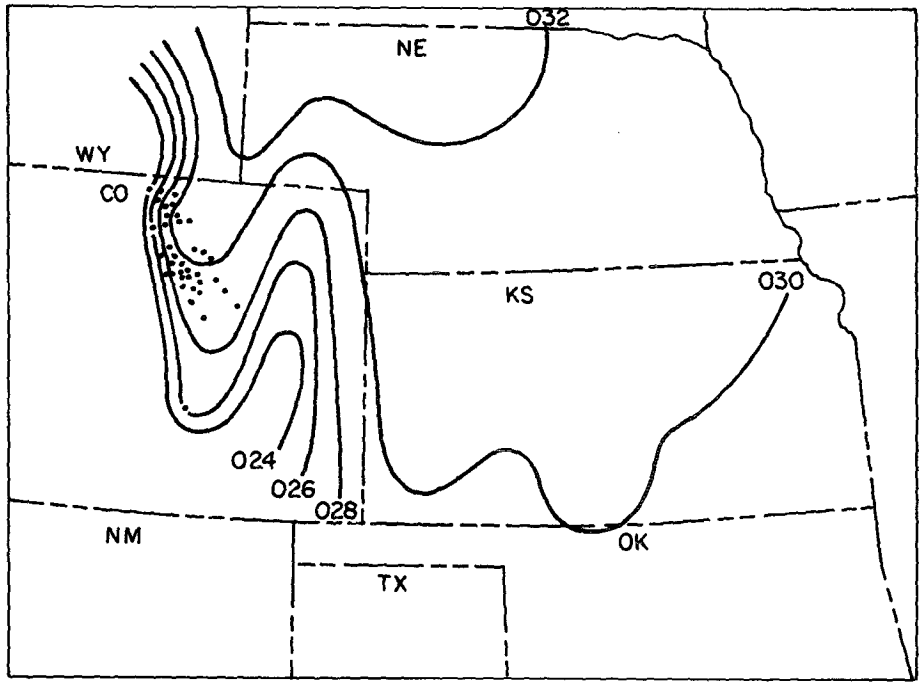

FIG. 16. As in Fig. 11, except an average for the period 1700 UTC 1 August 1986–1600 UTC 2 August 1986. Dots are plotted at locations of large hail reports on the afternoon of 2 August 1986.

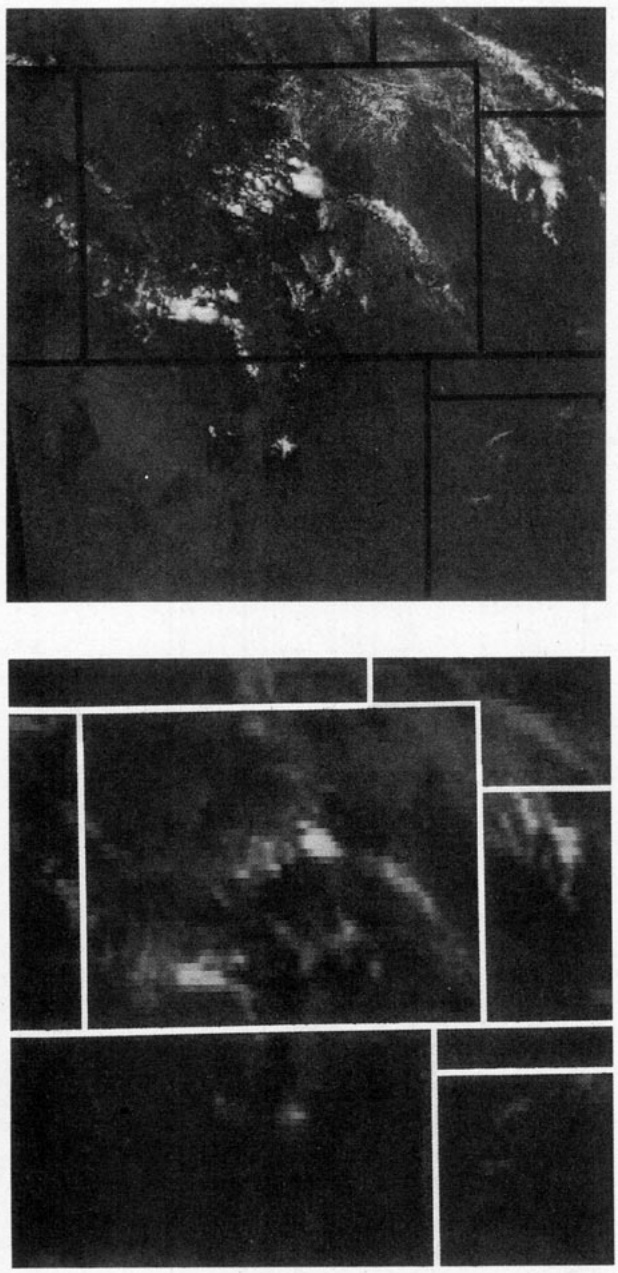

FIG. 17. (a) Visual and (b) infrared wavelength satellite imagery at 1800 UTC 2 August 1986 centered on Colorado.

high moisture content along the foothills in northern CO. It is even possible that the moisture source was, at least in part, the MCS activity from the previous day. Whether or not the latter is true, the deep moist layer produced a meso-β region of potentially unstable air which remained suppressed until late afternoon.[1] It was on the "high-terrain" side of this region where 95% of the severe weather occurred. The persistent mesoscale ridge in this region was identified through a careful analysis of the available surface data in conjunction with satellite imagery.

Acknowledgments. Both authors were supported at Colorado State University by the Cooperative Institute for Research in the Atmosphere through NOAA Grant NA-85-RAH-05045. Comments by Dr. R. H. Johnson, Dr. James Purdom, Dr. Charles Doswell as well as anonymous reviewers were extremely helpful in clarifying the main points of the analysis technique and the case study.

APPENDIX

Derivation of Pressure Adjustment

A modification of Sangster's procedure for observed data is developed in detail in this Appendix. The primary advantages of this new technique are that 1) it is not necessary to specify arbitrary conditions along the boundary of the analysis, and 2) the streamfunction analysis can be optimized to fit as closely as possible to the true geostrophic wind within a mesoscale air mass. The notation generally follows S87, and is based on the widespread practice of using altimeter settings to construct a surface mesoscale pressure analysis:

Z	geopotential height
Z_p	pressure height in the standard atmosphere
D	$[=Z - Z_p]$ altimeter correction (often referred to as the D-value)
T_v	virtual temperature
T_p	standard atmosphere temperature at the height $\{Z_p\,[=288.15 - (0.0065Z_p)$; SI units$]\}$
S^*	$[=(T_v - T_p)/T_p]$ fractional deviation of the temperature from standard (the inverse of the density deviation from standard)
D'	adjusted D-value [defined by (A2)]
Z'	arbitrary pressure height used to adjust D-values
S'	artificial S^* used to adjust a D-value
∇	horizontal gradient operator with derivatives evaluated along the ground
∇_p	horizontal gradient operator with derivatives evaluated on a constant pressure surface

Readers familiar with terrain-following coordinate systems used in numerical models may wish to refer to Davies-Jones for the correspondence between Pielke and Cram (1987) and S87.

[1] This suppression was inferred from spotter reports submitted by several qualified NOAA and Colorado State University meteorologists. In particular, one of the authors noted a thick field of stratocumulus-cloud cover (approximately "broken") racing westward toward the Front Range around noon. The observation is further substantiated by the satellite imagery at 1800 UTC (Fig. 17), which reveals an extensive area of low-level cloudiness in an apparently "capped," u-shaped area.

The S87 equations (3) and (6) are repeated here as

$$\nabla_p Z = \nabla D - S^* \nabla Z_p, \quad \text{(A1)}$$

and

$$D' = D - S'(Z_p - Z'). \quad \text{(A2)}$$

Equation (A1) states that the gradient of height on a constant pressure surface (proportional to the horizontal pressure-gradient force) is merely equal to the gradient of the altimeter correction, plus an adjustment factor due to density differences when actual conditions differ from the standard atmosphere. Note that even if the surface pressure (measured by D) does not change, the horizontal-pressure gradient ($\nabla_p Z$) does change if there are changes in the air density (S^*) along a sloping surface (Holton 1967). As discussed in section 2, the adjustment factor can be neglected if density deviations (S^*) are small, or if the terrain is relatively flat so that the gradient of surface pressure (∇Z_p) is small. Otherwise, the adjustment factor cannot be ignored. For example at latitude 40°, given a slope of 200 m/100 km and with an atmosphere that is merely 10 K warmer or colder than standard, the magnitude of the error in the geostrophic wind calculated from an analysis of raw altimeter settings is 7.3 m s^{-1}. The goal, according to (A2), is to determine adjusted D-values. The adjusted values depend on S', which in turn depends on S^* and on the terrain. Ideally, an analysis of D' would satisfy

$$\nabla D' = \nabla_p Z \quad \text{(A3)}$$

at every point on the ground. In an attempt to meet the desired condition (A3), both Z' and the field of S' can be adjusted.[2]

Unfortunately, there is no D' field that can satisfy (A3) everywhere as long as contours of density deviations (S^*) intersect contours of terrain height. In that case, as discussed by S87, Doswell (1988), and Davies-Jones (1988), there is a thermal wind parallel to the gradient of terrain height. This means that streamlines of the geostrophic wind at higher elevations are not the same as those at lower elevations, and so there is divergence in the surface geostrophic wind. The geostrophic wind simply does not remain nondivergent when projected from the sloping terrain onto a flat pressure surface.

S87 and Pielke and Cram (1987) avoid contending directly with the impossible requirements of (A3), instead defining D' as a solution to

$$\nabla^2 D' = \nabla_p{}^2 Z. \quad \text{(A4)}$$

The extent to which D' also satisfies (A3) depends on the choice of boundary conditions, which determine the partitioning of the true geostrophic wind between divergent and rotational components. It is possible to make the divergent component vanish at one or several points, but the divergence itself cannot be eliminated. Analogous to projecting the surface of the spherical earth onto a flat map, the analysis can be true only at certain points or along certain lines. Our philosophy, for a mesoscale analysis, is to return to (A2)–(A3), abandoning boundary conditions, and to minimize over a small portion of the analysis area the discrepancy between the streamfunction analysis and the geostrophic wind. The technique described below departs from S87 in the method for determining appropriate values of S'.

There is an exact relationship between S^* and S' when the contours of S^* are parallel to the terrain height contours. Although such a special condition is seldom observed, this idealization is a starting point for the approximate analyses that are normally required. For now assume that S^* depends only on Z_p as follows:

$$S^* = \alpha + \beta(Z_p - Z') + \gamma(Z_p - Z')^2 + \cdots. \quad \text{(A5)}$$

For this special case there is only one correct solution for S':

$$S' = \alpha + (1/2)\beta(Z_p - Z') + (1/3)\gamma(Z_p - Z')^2 + \cdots. \quad \text{(A6)}$$

Equation (A6) can be verified by substituting it into (A2) yielding

$$D' = D - [\alpha(Z_p - Z') + (1/2)\beta(Z_p - Z')^2 + (1/3)\gamma(Z_p - Z')^3 + \cdots], \quad \text{(A7)}$$

which automatically satisfies (A3) and (A4) at all points. Boundary conditions should not be specified independently.

Although there are some analogies with the conventional reduction of pressure to sea-level, it bears emphasizing that for this special condition, (A6) and (A7) yield the exact horizontal pressure gradient at the earth's surface, not at some level separated from the surface by a hypothetical column of air. Unlike conventional sea level pressure, the terrain slope as well as the gradients of S^* have been taken into account. It is best to regard S' and Z' simply as intermediate steps to obtaining the horizontal pressure gradient at the surface. For this special case, S' can be defined as

$$S'(Z_p) = \frac{\int_{Z_p}^{Z'} S^* \, dZ}{Z' - Z_p} \quad \text{(A8)}$$

with the integral evaluated along the sloping surface of the ground.

[2] In contrast, sea-level pressure essentially involves setting $Z' = 0$, with S' at each station approximately an average of the current S^* and the S^* for 12 hours earlier. Additionally, a plateau correction generally reduces the magnitude of S' over high terrain.

Contours of S^* do, in fact, normally intersect terrain contours, and this introduces errors in the analysis. However, it is always possible to approximate the observed S^* with an S^* that depends only on Z_p. There will be errors in areas where there is a difference between the actual and the approximate S^*, but the location and magnitude of these differences can be controlled by the analyst, perhaps interactively in a real-time operational setting. One of the advantages of this modified technique is that Z' can be located at an intermediate level within the analysis area. In contrast, the S87 technique requires that Z' be located either above the highest point or below the lowest point in the analysis area. This restriction reduces the potential accuracy of the analysis near intermediate levels.

Using an S' that depends only on elevation has the advantage that the up- or downslope component of the geostrophic wind is indicated correctly at all points by the ADJALT analysis. This is because the amount of adjustment is identical for stations which are at the same elevation. The unavoidable divergent component of the geostrophic wind is contained entirely in the other direction—the direction parallel to the terrain height contours. At times it may be desirable to have a better estimate in this direction (i.e., it may be desirable to have a better estimate of the pressure gradient directed towards or away from higher terrain). This is the motivation for adjustment method 2 (M2) discussed in section 3d. Other methods could be devised for different regions or different weather patterns. The final test for any method is how well it approximates the horizontal-pressure difference between any two stations (Fig. 2a) in the area of interest.

The D-value is usually reported in surface observations as an altimeter setting (i.e., the ALT is the pressure in the standard atmosphere at a height of negative D). The following simple formula for determining D (m) from ALT (inches Hg) is given in S87:

$$D = 281.7\,(\mathrm{ALT} - 29.92) - 4.49\,(\mathrm{ALT} - 29.92)^2. \tag{A9}$$

The derivative of (A9) yields

$$(\Delta D/\Delta \mathrm{ALT}) = 281.7 - 8.98\,(\mathrm{ALT} - 29.92). \tag{A10}$$

To a good approximation $(\Delta D/\Delta \mathrm{ALT})$ is a constant. There is, however, a small contribution from the final term in (A10). We used an average value for ALT (30.20) within northeast CO in this final term. Finally, note that because the ALT is an alternative way to express the surface D-value, the gradient of ADJALT is analogous to the height gradient on a constant-pressure surface. Converting from the ADJALT gradient to the horizontal pressure gradient force is simply a matter of multiplying by a constant; there is no dependence on variable density.

REFERENCES

Bellamy, J. C. 1945. The use of pressure altitude and altimeter corrections in meteorology. *J. Meteor.* **2**: 1–79.

Cram, J. M., and R. A. Pielke. 1989. Further comparison of two synoptic surface wind and pressure analysis methods. *Mon. Wea. Rev.* **117**: 696–706.

Danard, M. B. 1989. On computing the surface horizontal pressure gradient over elevated terrain. *Mon. Wea. Rev.* **117**: 1344–1350.

Davies-Jones, R. 1988. On the formulation of surface geostrophic streamfunction. *Mon. Wea. Rev.* **116**: 1824–1826.

Doswell, C. A. 1980. Synoptic-scale environments associated with High Plains severe thunderstorms. *Bull. Amer. Meteor. Soc.* **61**: 1388–1400.

——. 1988. Comments on "An improved technique for computing the horizontal pressure-gradient force at the earth's surface". *Mon. Wea. Rev.* **116**: 1251–1254.

Garratt, J. R., and W. L. Physick. 1987. Numerical study of atmospheric gravity currents. II: Evolution and external influences. *Contrib. Atmos. Physics* **60**: 88–103.

Holton, J. R. 1967. The diurnal boundary layer wind oscillation above sloping terrain. *Tellus* **19**: 199–205.

Mass, C. F., and M. D. Albright. 1987. Coastal southerlies and alongshore surges of the west coast of North America: Evidence of topographically trapped response to synoptic forcing. *Mon. Wea. Rev.* **115**: 1707–1738.

McAnelly, R. L., and W. R. Cotton. 1986. Meso-β scale characteristics of an episode of meso-α scale convective complexes. *Mon. Wea. Rev.* **114**: 1740–1770.

Pielke, R. A., and J. M. Cram. 1987. An alternate procedure for analyzing surface geostrophic winds and pressure over elevated terrain. *Wea. Forecasting* **2**: 229–236.

Purdom, J. F. W. 1982. Subjective interpretation of geostationary satellite data for nowcasting. In *Nowcasting*, K. A. Browning, ed., New York: Academic Press.

Richwien, B. A. 1980. The damming effect of the southern Appalachians. *Nat. Wea., Digest* **5**: 2–12.

Sangster, W. E. 1987. An improved technique for computing the horizontal pressure-gradient force at the Earth's surface. *Mon. Wea. Rev.* **115**: 1358–1369.

Storm Data. 1986. Vol. 28(8): NOAA/NESDIS publication, National Climatic Data Center, Asheville, NC 28801.

Toth, J. J., and R. H. Johnson. 1985. Summer surface flow characteristics over northeast Colorado. *Mon. Wea. Rev.* **113**: 1458–1469.

Weaver, J. F., and J. M. Brown. 1982. Forecasting an unusual weather event in Colorado: 15 October 1980. *Bull. Amer. Meteor. Soc.* **63**: 1142–1150.

——, and S. P. Nelson. 1982. Multiscale aspects of thunderstorm gust fronts and their effects on subsequent storm development. *Mon. Wea. Rev.* **110**: 707–718.